Estimation of bulk viscosity of dilute gases using a nonequilibrium molecular dynamics approach

Bhanuday Sharma and Rakesh Kumar*
Indian Institute of Technology Kanpur, Uttar Pradesh, India 208016

(Received 27 March 2019; revised manuscript received 3 June 2019; published 24 July 2019)

A method is proposed for the calculation of bulk viscosity, μ_b, of dilute gases using nonequilibrium molecular dynamics (NEMD) simulations. The method uses measurement of mechanical (P_{mech}) and thermodynamic pressure (P_{thermo}) in a NEMD simulation of an expanding fluid and then relates the bulk viscosity to them by the relation $\mu_b = (P_{\text{mech}} - P_{\text{thermo}})/\nabla \cdot \vec{u}$, where $\nabla \cdot \vec{u}$ is the controlled rate of expansion of the fluid per unit volume. A special emphasis is given to the fundamental physical understanding of bulk viscosity in this work. The proposed method is demonstrated for the estimation of bulk viscosity of dilute nitrogen gas in the temperature range of 200–800 K. Variation of bulk viscosity with temperature is reported in the above-mentioned temperature range and is found to be in a reasonably good agreement with the data available in the literature. Furthermore, variation of bulk viscosity with pressure and volumetric expansion rate is obtained. A weak linear dependency of bulk viscosity with pressure is observed, which increases with temperature. However, no significant effect of the rate of volumetric expansion is observed until 10^8 s^{-1}. Moreover, the effect of the direction of volumetric change (expansion vs. compression) is also demonstrated in this work.

DOI: 10.1103/PhysRevE.100.013309

I. INTRODUCTION

Ever since Sir George Gabriel Stokes (1819–1903) proposed the complete set of equations for the dynamics of viscous fluids in 1845 [1], bulk viscosity has remained as one of the most controversial subjects of fluid dynamics [2]. The recent surge of interest in Mars missions has made the study of bulk viscosity more relevant, as the Martian atmosphere consists approximately 96% of carbon dioxide gas, which has the bulk-to-shear-viscosity ratio $\approx$2000 [3,4]. The account of bulk viscosity in the analysis has also enabled more accurate modeling of several fluid mechanical phenomena [5–17]. On the other hand, in contrast to shear viscosity, which is a very well studied subject, the field of bulk viscosity is still not completely explored. There are considerable ambiguities about the nature, effects, and applicability of the concept of bulk viscosity. Even for most common fluids, existing experimental values of bulk viscosity are spread over a broad range, and widely accepted values are still not available [18]. In this paper, we provide a detailed physical insights on concept of bulk viscosity of dilute gases and propose a method for its calculation using nonequilibrium molecular dynamics approach.

The stress-strain rate relationship (i.e., constitutive relation) for a Newtonian fluid is given as follows:

$$\sigma_{ik} = -P_{\text{thermo}}\,\delta_{ik} + \mu\left(\frac{\partial u_i}{\partial x_k} + \frac{\partial u_k}{\partial x_i}\right) + \lambda\frac{\partial u_j}{\partial x_j}\delta_{ik}, \quad (1)$$

where σ_{ik} is Cauchy's stress tensor, δ_{ik} is the Kronecker delta, u_i is velocity of the fluid, x_i is a spatial coordinate, and the scalar quantity P_{thermo} is the thermodynamic pressure or hydrostatic pressure. The above relation contains two independent coefficients; the first is the coefficient of shear viscosity (μ), which is sometimes also termed as the first coefficient of viscosity, and the second is the coefficient of longitudinal viscosity (λ), which is also referred to as the second coefficient of viscosity.

The above relation, Eq. (1), can be rearranged as follows by separating isotropic and deviatoric parts of the strain-rate tensor:

$$\sigma_{ik} = -P_{\text{thermo}}\,\delta_{ik} + \mu\left(\frac{\partial u_i}{\partial x_k} + \frac{\partial u_k}{\partial x_i} - \frac{2}{3}\frac{\partial u_j}{\partial x_j}\delta_{ik}\right) + \mu_b\frac{\partial u_j}{\partial x_j}\delta_{ik}, \quad (2)$$

where $\mu_b = (\frac{2}{3}\mu + \lambda)$. The coefficient μ_b is known as the coefficient of bulk viscosity, and it represents the irreversible resistance, over and above the reversible resistance, caused by isentropic bulk modulus to change of volume [19]. Its values are expressed in the same units as shear viscosity, i.e., Pa s or poise. Thermodynamics constrains both the shear viscosity and bulk viscosity to have only non-negative values [20]. The values of bulk viscosity for common dilute gases at 300 K are listed in Table I [21]. It should be noted that the bulk viscosity of dilute monatomic gases is zero.

The mechanical pressure, P_{mech}, is defined as the negative average of the diagonal terms of stress tensor, as given below:

$$P_{\text{mech}} = -\tfrac{1}{3}(\sigma_{11} + \sigma_{22} + \sigma_{33}) = P_{\text{thermo}} - \mu_b\,\nabla \cdot \vec{u}. \quad (3)$$

Historically, Stokes [1] assumed the bulk viscosity (μ_b) to be identically zero for all fluids. It implies that mechanical pressure is always equal to thermodynamic pressure, irrespective of the process through which the system is undergoing, i.e.,

*Corresponding author: Associate Professor, Department of Aerospace Engineering; rkm@iitk.ac.in

TABLE I. Ratio of bulk viscosity to shear viscosity for common gases at 300 K [21].

Gas	μ_b/μ	Gas	μ_b/μ
Carbon monoxide	0.548	Dimethylpropane	3.265
Nitrogen	0.769	Water vapor	7.36
n-Pentane	0.896	Hydrogen	28.95
Isopentane	1.057	Chlorine	751.88
n-Butane	1.13	Fluorine	2329
Isobutane	2.00	Carbon dioxide	3828

the viscous forces do not depend on the rate of expansion or compression at all. This assumption is known as Stokes's hypothesis. Later, it became customary to use this hypothesis in fluid mechanics. However, Stokes [1] himself did not take this hypothesis as always true. He mentioned that in commonly encountered flows, if analysis with and without considering bulk viscosity produces the same results, then it would be because of small $\nabla \cdot \vec{u}$ rather than μ_b being zero. However, there are instances, where we cannot neglect the effects of bulk viscosity, for example, when the $\nabla \cdot \vec{u}$ is very high (e.g., inside a shock wave); when fluid is compressed and expanded in repeated cycles such that the cumulative effect of the small contribution from each cycle is no more negligible (e.g., sound wave) [22]; when the atmosphere consists of majority of those gases, such as CO_2, which exhibit a large bulk viscosity [5]; or when results of interest might get affected by even small disturbances, e.g., study of Rayleigh-Taylor instability [15]. In such cases, it becomes necessary to account for the bulk viscosity terms in the Navier-Stokes equation.

In addition to these classical hydrodynamics scenarios, bulk viscosity may also play an important role in several cosmological phenomena, e.g., damping of vibrations created during the formation of a new neutron star and growth of gravitational-wave instability in rapidly rotating neutron star [23,24]. The origin of bulk viscosity in these circumstances is primarily due to the chemical nonequilibrium caused by nuclear reactions. Bulk viscosity along with other transport properties is also of central importance to the space-time description of the heavy-ion collision experiments being conducted at the Brookhaven National Laboratory's Relativistic Heavy Ion Collider and CERN's Large Hadron Collider. One of the primary objectives of these experiments was the formation and investigation of quark-gluon plasma (QGP), the state of the matter of the Early Universe (first 30 μs after the Big Bang) [25].

In all these applications, precise values of bulk viscosity are needed, and to develop a method for its estimation is the primary aim of this work.

The paper is organized as follows: In Sec. II, we first describe the physical mechanism responsible for the genesis of normal stresses in dilute gases due to both shear and bulk viscosity. In Sec. III, we review the existing methods available for the determination of bulk viscosity. Section IV outlines the proposed method and describes the intermolecular potential used in the molecular dynamics (MD) simulations. In Sec. V, the results of present MD simulations are presented and analyzed. Finally, concluding remarks are made in Sec. VI.

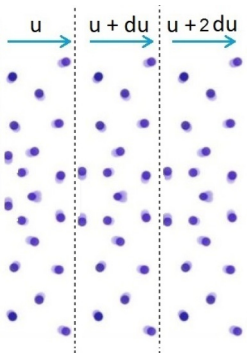

FIG. 1. Three layers of different velocity in a divergent flow field. Dots represent gas molecules and two vertical dashed lines are imaginary boundaries separating these three fluid layers.

II. MICROSCOPIC PICTURE OF NORMAL STRESSES IN AN EXPANDING OR CONTRACTING DILUTE GAS

To understand the microscopic origin of the normal stress, we rewrite Eq. (2) for the normal stresses acting in the x direction on the yz plane of the fluid element,

$$\sigma_{11} = -P_{\text{thermo}} + 2\mu\left(\frac{\partial u_1}{\partial x_1} - \frac{1}{3}\nabla \cdot \vec{u}\right) + \mu_b \nabla \cdot \vec{u}. \quad (4)$$

The second and third terms in the above equation are contributions of shear and bulk viscosity to normal stress, respectively. Mechanisms responsible for stresses due to these terms are discussed as follows.

A. Shear viscosity

In dilute gases, the mechanism of generation of normal stress due to shear viscosity is analogous to the mechanism that produces shear stress, i.e., the transport of momentum in adjacent layers of fluid due to thermal diffusion of molecules. Consider a flow field dilating only in one direction with three different layers of fluid having velocities as shown in Fig. 1. The left, middle, and right layers have a bulk velocity equal to u, $u + du$, and $u + 2du$, respectively, in the direction as shown in Fig. 1. When any molecule from the leftmost layer jumps to middle layer due to its random thermal motion, it will decrease the average momentum of middle layer. As a result, the middle layer will be pulled toward the left side. Similarly, if any molecule from the rightmost layer jumps to the middle layer, then it will increase the average momentum of middle layer. As a consequence, there is a pull on the middle layer toward the right side. The combined effect of these two pulls will be a normal stress on the fluid element of middle layer along the direction of velocity gradient. Therefore, in contrast to what the name "shear viscosity" can misrepresent, shear viscosity can produce not only shear stresses but also normal stresses.

B. Bulk viscosity

Herzfeld and Rice [26] first suggested that microscopic cause of bulk viscosity is the slow exchange of energy between the translational mode and internal degrees of freedom (viz., rotational and vibrational). The mechanism can be

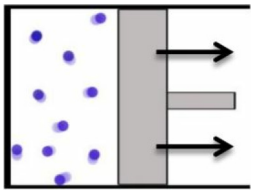

FIG. 2. Expansion of gas in a piston-cylinder arrangement.

explained by considering a simple example in which a polyatomic dilute gas, say, nitrogen, is expanding adiabatically in a piston-cylinder arrangement, as shown in Fig. 2.

Let us assume that initially the piston was at rest, and the gas was in equilibrium at a temperature of 300 K. With the assumption of frozen vibrational mode at the prevailing temperature conditions, the gas has three translational and two rotational degrees of freedom. Since the gas is in equilibrium, these all five degrees of freedom possess equal amount of energy because of the equipartition law of energy. Now, when the gas expands, it does work against the piston and loses its energy. The energy that the gas loses comes directly from its translational mode, whereas the energy associated with rotational mode remains momentarily unaffected. It causes an imbalance in the equipartition of energy among translational and rotational degrees of freedom. At this stage, the system is in a state of nonequilibrium, and its current translational kinetic energy is less than that which would be if the system is again brought to equilibrium adiabatically. Similarly, its rotational kinetic energy is more than that which would be if the system is brought to equilibrium. The system tries to regain its state such that the whole kinetic energy is equally distributed among all degrees of freedom. In this attempt, the system transfers some of its kinetic energy from internal modes to translational modes by means of intermolecular collisions among gas molecules.

The mechanical pressure, P_{mech}, at any point in the fluid is the negative average of normal stresses acting on that point. For a dilute gas, it represents actual force caused by bombardment of molecules on a unit area and therefore depends only on the random translational kinetic energy of the gas molecules. This is also the reason why PV work comes at the cost of translational kinetic energy. Kinetic theory of gases relates mechanical pressure to translational kinetic energy (E_{trans}) by the following relation:

$$P_{\text{mech}} = \frac{2\,E_{\text{trans}}}{3\mathcal{V}}, \tag{5}$$

where $\mathcal{V}$ is volume of the system. Hydrostatic or thermodynamic pressure, P_{thermo}, is the mechanical pressure of the system under hydrostatic conditions and, hence, equilibrium conditions. Therefore, for a system in nonequilibrium, the term "thermodynamic pressure" loses its meaning [20]. However, for such a system, it can still be defined as the mechanical pressure of the system if it is brought to equilibrium adiabatically [27]. Moreover, due to the equipartition law of energy, the translational kinetic energy (E_{trans}) of the system at equilibrium is equal to $3/f$ of the total energy (E_{total}), where f is number of total degrees of freedom of gas. Thus, the thermodynamic pressure can be given as follows:

$$P_{\text{thermo}} = \frac{2}{3\mathcal{V}}(E_{\text{trans}} \text{ at equilibrium}) = \frac{2}{3\mathcal{V}}\left(\frac{3}{f}E_{\text{total}}\right), \tag{6}$$

$$P_{\text{thermo}} = \frac{2\,E_{\text{total}}}{f\mathcal{V}}. \tag{7}$$

From the above discussion, it can be deduced that for the time duration, when translational kinetic energy is less than its value at equilibrium, the mechanical pressure is also less than the mechanical pressure at equilibrium (i.e., the thermodynamic pressure). Since monatomic gases do not possess any internal degrees of freedom, it becomes immediately clear that the mechanical pressure at any instant will always be equal to the thermodynamic pressure. Therefore, we can expect them to exhibit zero bulk viscosity if we consider the possibility of nonequilibrium in rotational and vibrational mode only. Both theories and experiments [28,29] also confirm the same.

However, it is possible that factors other than rotation and vibration, like electronic excitation or chemical reaction [20], can also cause nonequilibrium in monatomic gases. For instance, Istomin *et al.* [30] has shown that the bulk viscosity is not zero in electronically excited monatomic gases at temperatures higher than 2000 K. Similarly, if we consider the nonequilibrium within the translational degrees of freedom, i.e., among the X, Y, and Z directions of translational velocity, then also the monatomic gases can show nonzero bulk viscosity. However, the relaxation time of this kind of nonequilibrium is much smaller than the rotational-translational and vibrational-translational relaxation times [31]. Therefore, the contribution of such nonequilibrium processes to bulk viscosity is also small.

III. METHODS FOR DETERMINATION OF BULK VISCOSITY

Unlike shear viscosity, determination of bulk viscosity has always remained a challenging task. We present a brief summary of various approaches available for estimation of bulk viscosity, μ_b, of QGP and hadronic matter, and nonrelativistic classical fluids in Secs. III A and III B, respectively, with a particular focus on the latter.

A. Determination of bulk viscosity of QGP and hadronic matter

For the estimation of transport coefficient of QGP and hadronic matter, two standard approaches are mainly used: the Boltzmann equation-based relaxation time approximation (RTA) approach and the linear response theory-based Green-Kubo formulation. A brief review of these methods can be found in Refs. [25,32,33]. A vast amount of research has been done on this topic. Here we summarize only some of the key contributions in this field. Gavin [34] used the well-known nonrelativistic form of the Boltzmann equation to calculate the transport coefficients for both the QGP and hadronic matter using the RTA method. Prakash *et al.* [35,36] studied the equilibration of hot hadronic matter in the framework of relativistic kinetic theory. They calculated transport coefficients considering only elastic collisions in the dilute gas limit using extended Chapman-Enskog formalism. For a

general review of the relativistic kinetic theory, the reader may refer to the classical text by Groot *et al.* [37]. Chakraborty *et al.* [38] extended the classical works of Prakash *et al.* [35,36] and Gavin [34] and presented a theoretical framework for the calculation of shear and bulk viscosity of hot hadronic matter. Their work accounted for not only inelastic collisions but also formation and decay of resonances, temperature-dependent mean fields, and temperature-dependent masses. Demir *et al.* [25,39,40] carried out ultrarelativistic quantum molecular dynamics simulations of hadronic media and calculated bulk viscosity using both Green-Kubo method and relaxation time approximation.

B. Determination of bulk viscosity of classical fluids

1. Theoretical methods

Theoretically, bulk viscosity of dilute gases can be related to the relaxation time of equilibration processes by Tisza's [3] formulation, given as follows:

$$\mu_b = \rho_{\rm eq}\, a^2\, \frac{(\gamma-1)}{\gamma} \sum_i \frac{c_{v,i}}{c_v}\tau_i, \tag{8}$$

where $\rho_{\rm eq}$ is density of gas at equilibrium, a is speed of sound in absence of viscosity, γ is the ratio of specific heats at equilibrium, $c_{v,i}$ is heat capacity of ith internal mode, c_v is total heat capacity of the gas, and τ_i is the relaxation time of that internal mode, and the summation is performed over all internal degrees of freedoms (i.e., rotational, vibrational). However, the applicability of this expression is limited to the low-frequency regime where $\omega\tau \ll 1$, with ω being the frequency of sound wave [41].

Li *et al.* [42] related bulk viscosity to bulk modulus and relaxation time as follows:

$$\mu_b = K\tau_{\rm tot}, \tag{9}$$

where K is bulk modulus of the fluid, defined as $K = -\mathcal{V}(\partial P/\partial\mathcal{V})$, and $\tau_{\rm tot}$ is total average relaxation time of internal energy in all excited modes.

2. Experimental methods

The experimental determination of bulk viscosity is not as straightforward as shear viscosity and usually based on indirect techniques, such as absorption and dispersion of sound wave, and Rayleigh-Brillouin scattering [19,43,44].

Absorption of the sound wave is the additional decrease in intensity with distance, over and above the geometric reduction caused by the inverse square law. It has been found that the experimentally observed absorption is much higher than the predictions based on the theory that accounts only for classical absorption, i.e., absorption due to shear viscosity, thermal conductivity, and thermal radiation. Since this excess absorption cannot be attributed to dissipation phenomenon because of translational motion of molecules (i.e., shear viscosity, heat conduction), it is assumed that this excess absorption is because of bulk viscosity [45]. The absorption of sound is characterized by absorption coefficient (α), and it is related to bulk viscosity, μ_b, as follows [28]:

$$\frac{\alpha P_{\rm eq}}{\omega^2} = \frac{2\pi^2}{\gamma a}\left[\frac{4}{3}\mu + \frac{(\gamma-1)^2}{\gamma}\frac{M\kappa}{R} + \mu_b\right], \tag{10}$$

where $P_{\rm eq}$ is equilibrium pressure, M is molar mass, κ is thermal conductivity, and R is gas constant.

However, the assumption that the excess absorption is due to bulk viscosity can only be examined when some direct measurements of bulk viscosity from an independent method are made and values are compared [4,45]. Furthermore, this approach of measuring bulk viscosity is susceptible to considerable errors since it involves subtraction of classical absorption coefficient from total absorption coefficient to get absorption due to bulk viscosity. For the calculation of classical absorption, the use of μ and κ taken from different sources also introduces error in estimates of bulk viscosity made using this method [44].

Alternatively, bulk viscosity can also be measured by sound dispersion experiments. Dispersion of sound causes speed of sound to be frequency dependent, and this dependency is given as follows [46]:

$$a^2 = a_0^2 + \left(a_\infty^2 - a_0^2\right)\frac{\omega^2\tau^2}{1+\omega^2\tau^2}, \tag{11}$$

where a is the speed of sound at frequency ω, a_0, and a_∞ are speed of sound for very low and very high frequencies, respectively. The obtained relaxation time then can be related to bulk viscosity.

Pan *et al.* [47] suggested that bulk viscosity of dilute gases can also be measured using coherent Rayleigh-Brillouin scattering. In this technique, gas density perturbations are generated and measured using laser beams. The experimentally observed scattering profile is then compared with that obtained from the theoretical models to get transport coefficients, including bulk viscosity. However, in contrast to acoustic experiments, which measure bulk viscosity at megahertz frequencies, these experiments measure bulk viscosity in gigahertz domain. Because of this reason, a significant difference between the estimated values from the two above-mentioned methods is usually observed [47–53].

Emanuel *et al.* [7] has deduced that for dense polyatomic gases, the density-based thickness of shock wave consists of many thousands of mean free paths and varies linearly with the ratio μ_b/μ. Thus, the experimentally measured shock wave thickness can be used to calculate bulk viscosity; nevertheless, we could not find any experimental implementation of this technique in the literature.

3. Computational methods

Numerical simulation methods used for estimation of bulk viscosity are classified into two categories, viz., equilibrium molecular dynamics– (EMD) based methods and nonequilibrium molecular dynamics– (NEMD) based methods. In the former, the system is first brought to thermodynamic equilibrium, and then transport coefficients are calculated by sampling the microscopic data. There are two such methods: the Green-Kubo method and Einstein's method. Both use the integrals of time-correlation functions of fluctuations of the pressure tensor to calculate shear and bulk viscosities.

The Green-Kubo method uses the Green-Kubo relations for calculation of transport properties [54,55]. For shear viscosity, μ, and bulk viscosity, μ_b, these relations are given as

follows:

$$\mu = \frac{\mathcal{V}}{k_B T} \int_0^\infty \langle P_{ij}(t)\, P_{ij}(0)\rangle dt, \tag{12}$$

where k_B is the Boltzmann constant, T is temperature, $P_{ij}(t)$ denotes the instantaneous value of the ijth off-diagonal element of the pressure tensor at a time t, and the angle bracket indicates the ensemble average. Further, to reduce the statistical error in calculation of μ, averaging is performed over three different values obtained from three different components of pressure tensor, viz., P_{ij}, P_{jk}, and P_{ki},

$$\mu_b = \frac{\mathcal{V}}{k_B T} \int_0^\infty \langle \delta P(t)\, \delta P(0)\rangle dt. \tag{13}$$

Here $P(t)$ is the instantaneous value of the average of three diagonal terms of pressure tensor at a time t, i.e., $P(t) = \frac{1}{3}[P_{ii}(t) + P_{jj}(t) + P_{kk}(t)]$. The fluctuations, $\delta P(t)$, is aberration of mean pressure from equilibrium pressure, i.e., $\delta P(t) = P(t) - P_{\rm eq}$, where $P_{\rm eq}$ is equilibrium pressure of the system, and it is calculated by the time average of $P(t)$ over a long time.

The EMD-based methods predict transport coefficient very well for most of the systems. However, in some cases, they suffer from several issues. For example, in the Green-Kubo method, for the correct estimation of viscosity coefficients, the autocorrelation function should decay to zero with time. In such a case, the integral of autocorrelation function would reach a constant value. Nevertheless, it does not necessarily happen in practice. The autocorrelation function might show either long-time tails or fluctuations [56]. Further, viscosities should be estimated from the region of the graph of the integral vs. time, when it reaches a constant value. First, it is difficult to identify such a region, and, second, even if we can identify such a region, there will always be arbitrariness in the value of viscosity because of ambiguity in determining the cut-off time [56].

A NEMD-based method, which measures transport coefficients by directly measuring the gradient of the corresponding parameter, can possibly overcome these issues. Such methods are well developed for shear viscosity, heat conductivity, and mass diffusivity. However, for bulk viscosity, historically it has been seen that implementation of such a method is a challenging task. To the best of our knowledge, only one attempt has been made so far to use NEMD-based methods for the estimation of bulk viscosity. In this work, Hoover *et al.* [19] cyclically compressed and expanded the fluid in the following manner to produce measurable effects:

$$L/L_0 = 1 + \xi \sin(\omega t), \tag{14}$$

where L_0 is mean length, L is instantaneous length of the cubic simulation domain, ξ is strain amplitude, and ω is the frequency describing the linearized strain rate,

$$\dot{\epsilon} = \xi\omega \cos(\omega t). \tag{15}$$

As the linearized strain rate ($\dot{\epsilon}$) approaches zero, the authors expected the average pressure of the system to deviate from equilibrium pressure by $-3\xi\omega\mu_b \cos(\omega t)$. Also, if the deformation given by Eq. (14) takes place through the mechanism of external work, then the lost work due to irreversible heating will give rise to energy increase per cycle (the cycle time being $2\pi/\omega$), which is equal to $(2\pi/\omega)9\xi^2\omega^2\mu_b\mathcal{V}/2$. Based on the measurement of average pressure and rise in the energy of the system, the authors estimated bulk viscosity of a soft sphere fluid modeled with potential $\phi(r) = \epsilon(\sigma/r)^{12}$.

C. The proposed method

From the above discussion, it is clear that a direct method, either experimental or computational, to calculate bulk viscosity directly form isotropic continuous expansion or compression does not exist so far. Therefore, we take the opportunity to show that bulk viscosity can indeed be reliably calculated from Eq. (3) using nonequilibrium molecular dynamics approach. In the proposed method, $P_{\rm mech}$, and $P_{\rm thermo}$ of a fluid undergoing volume change with constant $\nabla \cdot \vec{u}$ are determined by translational and internal energy content of the gas using Eqs. (5) and (7) and are then used to evaluate the bulk viscosity using Eq. (3). Such a method will be of great interest as it will provide a deeper insight into the physics of the subject and will serve long-awaited validation of Eq. (3). This method will also substantiate the hypothesis that excess absorption of sound energy is due to bulk viscosity [45]. Although the proposed method is in principle applicable to all expansion or compression rates, a practical application of the method requires a sufficiently high expansion or compression rates (e.g., $\nabla \cdot \vec{u} \sim 10^8$ s^{-1} for N_2) to measure accurate values of bulk viscosity (see Sec. V D for more details).

The proposed approach differs from that of Hoover *et al.* in several aspects. First, Hoover *et al.* modified the Hamiltonian equation itself to simulate homogeneous compression and expansion with periodic boundaries. On the other hand, we have not made any kind of alteration in the equations of dynamics. Moreover, we have used reflective wall-type boundaries to make the expansion or compression (and hence, extraction (addition) of energy from (to) the system by means of work) more realistic. Therefore, the approach adopted in the present work is closer to the natural physics.

The second major difference is that Hoover *et al.* calculated bulk viscosity of a dense fluid by simulating point particles with a soft-sphere potential. Hence, they ignored the contribution in bulk viscosity arising from rotational and vibrational relaxation and accounted for only the contribution of structural rearrangement of molecules, which is significant only in case of dense fluids. In contrast to this, we have calculated bulk viscosity of a dilute gas accounting for the contribution of rotational relaxation. We have ignored the contribution of structural rearrangement of molecules by assuming that the pressure due to pairwise intermolecular interaction, $P_{\rm pair}$, is small.

IV. MOLECULAR MODEL AND EXPRESSIONS FOR PRESSURE CALCULATION

A. Molecular model

The classical MD models atoms as point mass objects and calculates their trajectory according to Newton's laws of motion. The word *classical* implies that the electronic structure and quantum mechanical effects are neglected. A brief overview of molecular dynamics approach can be found somewhere else [57,58]. In the present work, we have used the

Large Scale Atomic/Molecular Massively Parallel Simulator (LAMMPS) [59] to simulate dilute nitrogen gas. The nitrogen atoms are modeled as point particles interacting with each other as per the Lennard-Jones interatomic potential, given as follows:

$$V(r_{ij}) = \begin{cases} 4\epsilon\left[\left(\frac{\sigma}{r_{ij}}\right)^{12} - \left(\frac{\sigma}{r_{ij}}\right)^{6}\right], & \text{if } r_{ij} < r_{\text{cutoff}} \\ 0 & \text{if } r_{ij} > r_{\text{cutoff}} \end{cases},$$

where $\sigma = 3.17$ Å, $\epsilon = 0.0938$ kcal/mol, and $r_{\text{cutoff}} = 12$ Å [60]. The interamolecular N-N bond can be modeled as a harmonic oscillator (equilibrium bond length = 1.098 Å, and force constant = 2295 N/m) [61]. Moreover, the simulations are carried out in the temperature range 200–800 K. This temperature is quite low as compared to characteristic vibrational temperature of nitrogen ($\theta_v = 3374$ K [61]); therefore, it is assumed that the vibrational modes are not activated, i.e., there is no energy exchange taking place between vibrational and translational and vibrational and rotational modes [62]. We have implemented this constraint in our MD simulations by modeling N_2 molecule as a rigid rotor using RATTLE algorithm [63]. The RATTLE algorithm ensures that the distance between the atoms of a bond remain fixed, and the molecule behaves as a rigid rotor.

B. Expressions for pressure calculation

In general, stresses in any molecular dynamic system can be written as the summation of kinetic and virial term [64–66]. The virial term involves the contribution of pairwise interactions, long-range Coulombic interactions, etc. However, for a nonpolar dilute gas, as we show in Fig. 9 the virial term is small enough to be neglected. In this case, the expression for mechanical stress can be approximated by keeping only the kinetic term,

$$\sigma_{ab}\,\mathcal{V} = \sum_{1}^{N}(-m v_a v_b), \tag{16}$$

where σ_{ab} is component of stress tensor, where a and b take on values x, y, and z to generate σ_{xx}, σ_{yy}, σ_{zz}, σ_{xy}, σ_{yz}, and σ_{xz}; m is mass of the gas atom; v_a the component of velocity of the atom in the direction a; and N is total number of atoms. Hence, the expression of mechanical pressure can be written as

$$P_{\text{mech}} = -\left(\frac{\sigma_{xx} + \sigma_{yy} + \sigma_{zz}}{3}\right) = \frac{m\sum_1^N \left(v_x^2 + v_y^2 + v_z^3\right)}{3\mathcal{V}} = \frac{2\,E_{\text{trans}}}{3\mathcal{V}}. \tag{17}$$

If the system were in equilibrium with same total energy and volume, then the translational kinetic energy would have been $3/f$ of total energy. Thus, the expression for the thermodynamic pressure of a dilute diatomic gas, modeled as a rigid rotor, can be written as:

$$P_{\text{thermo}} = \frac{2\,E_{\text{total}}}{5\mathcal{V}}. \tag{18}$$

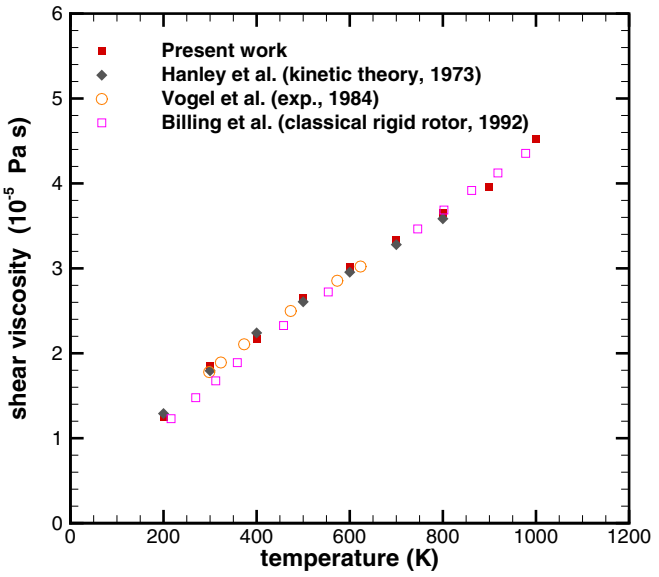

FIG. 3. Shear viscosity of nitrogen obtained from Green-Kubo formulation.

The component of pressure due to pairwise interaction, P_{pair}, is calculated as follows [66]:

$$P_{\text{pair}} = \frac{1}{6\mathcal{V}}\sum_{i=1}^{N}\sum_{j\neq i}^{N_p}(\vec{r}_i \cdot \vec{F}_{ij} + \vec{r}_j \cdot \vec{F}_{ji}), \tag{19}$$

where $\vec{r}_i$ and $\vec{r}_j$ are position vectors of ith and jth atom and $\vec{F}_{ij}$ is the force acting on ith atom due to its interaction with jth atom. First summation is performed over N_p neighbors of atom i, and second summation is performed over all the N atoms present in the simulation.

C. Expansion and compression

The expansion or compression is performed by displacing all the boundaries (outward for expansion and inward for compression) of the cubical domain, at every time step, by a distance δL, keeping centroid of the domain fixed,

$$\delta L = \frac{1}{2}\left(\frac{L\,\nabla\cdot\vec{u}}{3}\Delta t\right), \tag{20}$$

where L is instantaneous side of the cubical domain and Δt is time step size used in the simulation. The factor $1/2$ accounts for expansion or compression by displacement of both the opposite faces.

V. RESULTS AND DISCUSSION

A. Calculation of shear viscosity

To validate the molecular model of nitrogen (i.e., interatomic potential) that we have used to calculate bulk viscosity, we first calculated the shear viscosity of nitrogen with the Green-Kubo method. The results are shown and compared with the numerical works of Hanley *et al.* [67] and Billing *et al.* [68] and the experimental work of Vogel *et al.* [69] in Fig. 3. The close match between these results suggests that

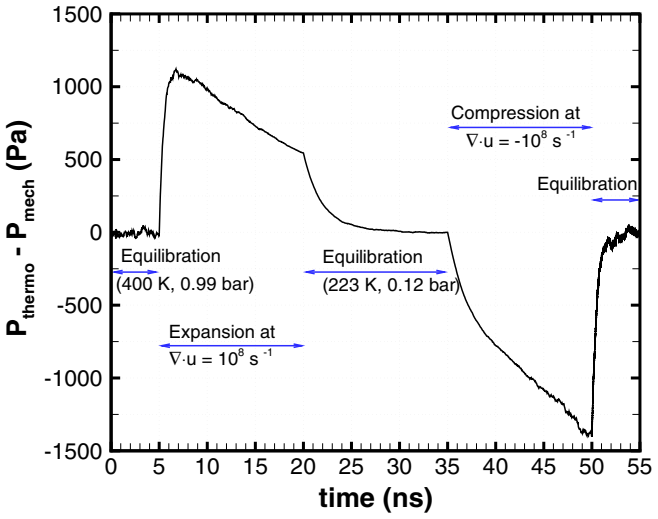

FIG. 4. Variation of $(P_{\text{thermo}} - P_{\text{mech}})$ in an expansion and compression with constant $\nabla \cdot \vec{u}$. The system was first subjected to equilibration from $t = 0$ to $t = 5$ ns ($\nabla \cdot \vec{u} = 0$), then expansion from $t = 5$ to $t = 20$ ns ($\nabla \cdot \vec{u} = 10^8\ \text{s}^{-1}$), again equilibration from $t = 20$ to $t = 35$ ns ($\nabla \cdot \vec{u} = 0$), compression from $t = 35$ to 50 ns ($\nabla \cdot \vec{u} = -10^8\ \text{s}^{-1}$), and finally again equilibration from $t = 50$ to 55 ns.

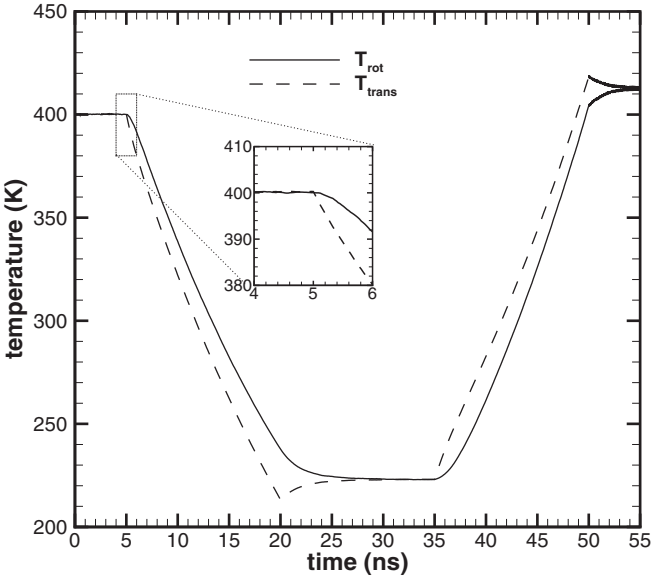

FIG. 5. Translational and rotational temperature variation. The inset shows enlarged view of region marked with dotted rectangle.

the chosen potential can reproduce thermodynamic properties of simulated gas within the acceptable limit of errors.

B. Demonstration of method through expansion of gas with constant $\nabla \cdot \vec{u}$

In this section, we show the implementation of homogeneous expansion technique to estimate bulk viscosity. For the simulations carried out in this work, it has been verified that the value of bulk viscosity does not get affected (within statistical uncertainty) by the time step size and the number of the molecules used in the simulation. A detailed analysis of the results, along with the physics of the problem, is presented as follows. First, a representative cubical fluid element, consisting of 3.85 million nitrogen molecules, is created. Boundaries of the simulation domain are modeled as the Lennard-Jones reflective wall. The molecules are first assigned velocities corresponding to a temperature and pressure of 400 K and 1 bar, respectively, and then the system is equilibrated for 5 ns. After that, it is adiabatically expanded with $\nabla \cdot \vec{u} = 10^8\ \text{s}^{-1}$. This expansion is further followed by another equilibration, and an adiabatic compression with same $|\nabla \cdot \vec{u}|$, and then a final equilibration. The above-mentioned process is shown in Fig. 4. The results are discussed as follows.

As shown in Fig. 4, initially, during the first equilibration, the value of $(P_{\text{thermo}} - P_{\text{mech}})$ oscillates about zero due to the exchange of energy between rotational and translational mode as the intermolecular collisions take place. It is ensured that the total energy of the system for this duration remains conserved within the numerical accuracy.

Then, at $t = 5$ ns, the system starts expanding and, hence, does work against the walls of the simulation domain. As we stated earlier, this work (energy) is extracted from translational kinetic energy (E_{trans}) of the gas and the kinetic energy associated with rotational mode (E_{rot}) remains as momentarily unaffected as the process of doing work does not affect the rotational mode directly. This statement can also be verified from Fig. 5, where the variation of translational and rotational temperature is shown with time. It can be observed that the slope of T_{trans} vs. time graph changes immediately at $t = 5$ ns; while the slope of T_{rot} vs. time remains zero beyond $t = 5$ ns, and after that, it changes gradually as the difference (ΔE) between $E_{\text{trans}}/3$ and $E_{\text{rot}}/2$ increases.

For a given thermodynamic state of the system, the rate of energy transfer from rotational to translational mode depends on the difference between translational and rotational temperature, ΔT. Initially, when the system is in a state of equilibrium, i.e., at $t = 5$ ns, the translational temperature is equal to the rotational temperature and hence ΔT is zero, as shown in Fig. 5. Now, as the expansion begins, the translational temperature starts decreasing immediately, whereas the rotational temperature instantaneously remains unchanged. This leads to a difference between the two temperatures (Fig. 5). Because of this difference, intermolecular collisions cause a net transfer of energy from rotational mode to translational mode. However, at this early stage, the difference ΔT is very small, and therefore the rate of decrease in E_{rot} (i.e., rate of energy transfer from rotational mode to translation mode) is also very small as compared to the rate at which system is losing its translational energy (i.e., rate at which system is doing work). So the ΔT further increases, as shown in Fig. 5. Consequently, rate of energy transfer from rotational mode to translational mode also increases.

After this transient phase of $t = 5$ to $\approx$10 ns (Fig. 4), the temperature difference ΔT and hence ΔP, both of which depend on the local thermodynamic state (i.e., temperature and pressure) of the system and expansion rate $\nabla \cdot \vec{u}$, reach their value corresponding to these conditions. At this stage, $(P_{\text{thermo}} - P_{\text{mech}})/\nabla \cdot \vec{u}$ can be considered as the value of bulk viscosity at the local thermodynamic state for the given value of $\nabla \cdot \vec{u}$. However, for the present case of adiabatic expansion

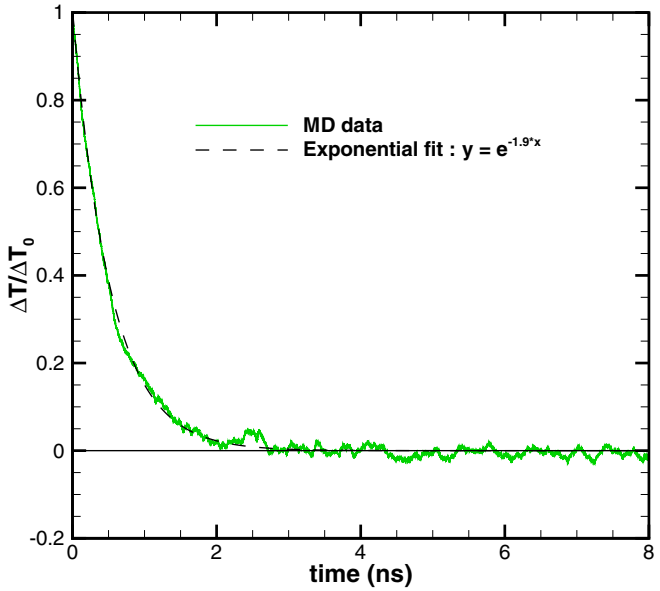

FIG. 6. Time history of $\Delta T/\Delta T_0$. It should be noted that the $t = 0$ ns of this figure corresponds to $t = 50$ ns of Fig. 4.

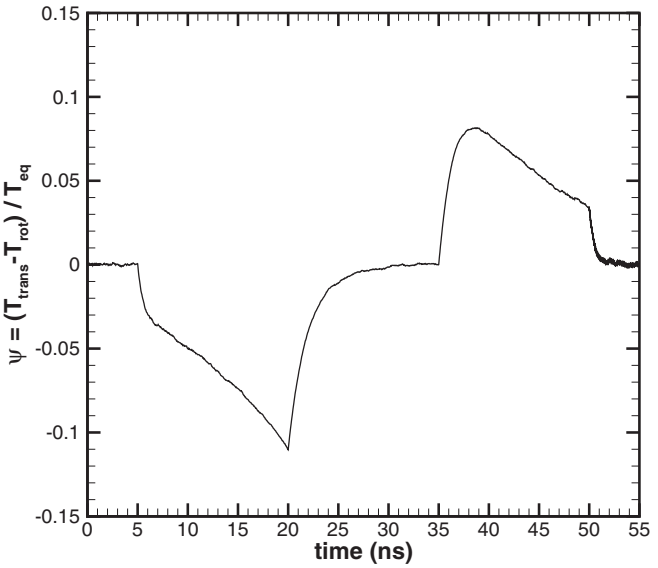

FIG. 7. Variation of nonequilibrium parameter, $\psi = (T_{\text{trans}} - T_{\text{rot}})/T_{\text{eq}}$, during the simulation

or compression, the temperature and pressure of the system are continuously changing. It results in continuously varying $(P_{\text{thermo}} - P_{\text{mech}})$ during $t = 10$ to 20 ns and $t = 40$ to 50 ns as shown in Fig. 4. Furthermore, the asymmetry of curve between the expansion and compression region of Fig. 4 is explained by the argument that the system requires some finite time to reach its pseudo steady state, along with the fact that $\mu_{b(\text{compression})} > \mu_{b(\text{expansion})}$ (see Sec. V D).

At $t = 35$ ns, the system is subjected to compression with $\nabla \cdot \vec{u} = -10^8$ s^{-1}. In a similar fashion to the expansion, $(P_{\text{thermo}} - P_{\text{mech}})$ or ΔP reaches a pseudo steady state in approximately 5 ns, i.e., at $t = 40$ ns, after which we can consider $(P_{\text{thermo}} - P_{\text{mech}})/\nabla \cdot \vec{u}$ to be equal to bulk viscosity.

Finally, at $t = 50$ ns, the compression is seized, and the system is allowed to return to its state of equilibrium. For this equilibration process, the variation of $\Delta T/\Delta T_0$ with time is plotted in the Fig. 6, where ΔT_0 is value of ΔT at $t = 50$. It should be noted that the $t = 0$ ns of Fig. 6 corresponds to $t = 50$ ns of Fig. 4. By fitting the curve of $\Delta T/\Delta T_0$ vs. time to an exponential curve $[\Delta T/\Delta T_0 = \exp(-t/\tau_{\text{rot}})]$, we calculated the rotational relaxation time (τ_{rot}) of the system. In this simulation we obtain a rotational relaxation time, $\tau_{\text{rot}} = 0.53$ ns for a compression rate $\nabla \cdot \vec{u}$ of -10^8 s^{-1}. We can also calculate the corresponding value of rotational relaxation number, which is given as $Z_{\text{rot}} = \tau_{\text{rot}}/\tau_c$, where the mean collision time (τ_c) is defined with its usual definition $\tau_c = \lambda/\bar{C}'$ and λ is the mean free path and $\bar{C}'$ is the mean molecular speed. We obtain $Z_{\text{rot}} = 3$ at a temperature and pressure of 412 K and 1.038 bar, respectively. This compares fairly well with the Z_{rot} range of 2 to 6 found in the literature [68,70–74]. The value of τ_{rot}, obtained during the equilibration process, can also be used to calculate bulk viscosity using the Tisza's formulation [Eq. (8)] [3]. For nitrogen with frozen vibrational levels, $C_{v_{\text{rot}}} = R$. Hence, Tisza's expression for bulk viscosity reduces to $\mu_b = (\gamma - 1)^2 P_{\text{eq}}\, \tau_{\text{rot}}$. This procedure yielded a bulk viscosity value of 9×10^{-6} Pa s, as compared to 1.3×10^{-5} Pa s at a temperature of 412 K and pressure of 0.96 bar, obtained by direct calculation based on the pressure difference between mechanical and thermodynamic pressure in our work. Noteworthy is the fact that the calculation of bulk viscosity through estimation of relaxation time by fitting the $\Delta T/\Delta T_0$ vs. t curve to exponential curve is very sensitive to curve fitting. Even for two different but equally good fit, there could be a huge variation in measured relaxation time and hence the bulk viscosity. On the other hand, a direct calculation of bulk viscosity from the difference between mechanical and thermodynamic pressure, as demonstrated in this work, is straightforward and free from such errors.

Another important point, which needs to be addressed, is that for the algorithm to work properly, the flow characteristic time should be greater than the relaxation time of internal mode or a near-thermodynamic equilibrium condition should prevail [75]. In other words, the expansion or compression shall be slow enough as compared to the internal energy collisional relaxation. To this end, if we take inverse of expansion rate, i.e., $(\nabla \cdot \vec{u})^{-1} = 10^{-8}$ s, as the flow characteristic time and compare it with the relaxation time, τ_{rot}, value of 5.3×10^{-10} s obtained previously, then it turns out that the condition is indeed satisfied. The further reduction of $\nabla \cdot \vec{u}$ to 10^7 s^{-1} has also not produced any significant change in μ_b. Details of this study are discussed in Sec. V D. Another reason to ensure the near-equilibrium condition is that the Z_{rot} and hence the relaxation rate is not only dependent on the near-equilibrium temperature but also the magnitude of nonequilibrium [31]. To quantify the deviation of simulated gas from equilibrium, we have plotted the variation of nonequilibrium parameter, $\psi = (T_{\text{trans}} - T_{\text{rot}})/T_{\text{eq}}$, with time, where T_{eq} is corresponding equilibrium temperature (Fig. 7). It can be seen that the $|\psi|$ remains less than 0.15 throughout the simulation, whereas the variation in Z_{rot} over this range of ψ is less than 0.1 [31]. Therefore, although at first $\nabla \cdot \vec{u}$ of the order of 10^8 s^{-1} may seem too high for the simulation to fall in the

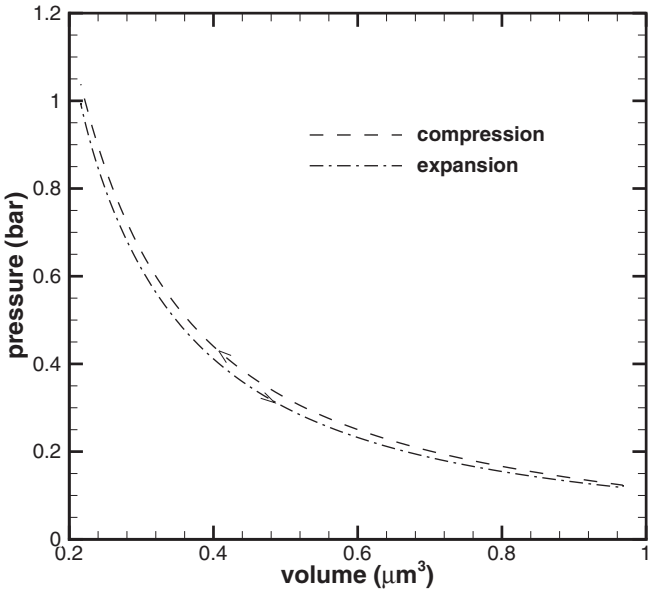

FIG. 8. Pressure vs. volume graph for simple expansion followed by a compression.

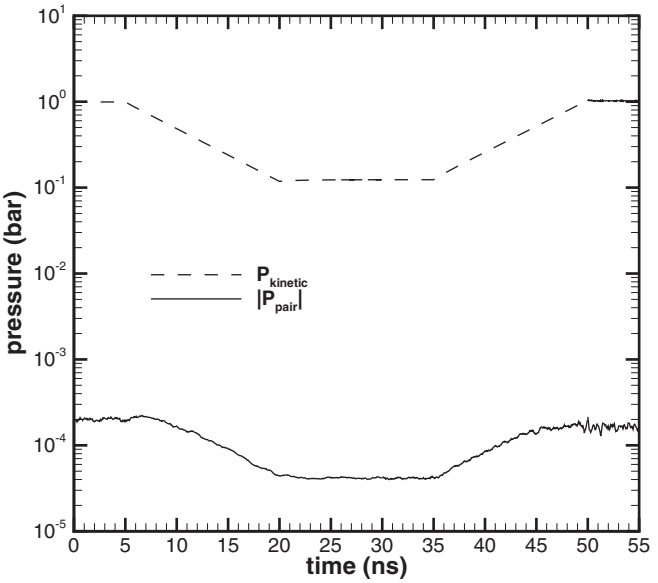

FIG. 9. Contribution of translational kinetic energy (P_{kinetic}) and pairwise interaction (P_{pair}) in calculation of mechanical pressure

"near-equilibrium" regime, the obtained range of ψ once again confirms that it is indeed a near-equilibrium simulation.

From another perspective, during the adiabatic expansion, the temperature and pressure of the gas continuously changes, hence the bulk viscosity, which is dependent on temperature and pressure of gas. Therefore, instantaneous value of $(P_{\text{thermo}} - P_{\text{mech}})/\nabla \cdot \vec{u}$ will be a fair approximation of μ_b only if change in bulk viscosity in a duration equal to one relaxation time is small enough so that the effects of continuously varying μ_b on $(P_{\text{thermo}} - P_{\text{mech}})$ can be neglected. Otherwise, before the $(P_{\text{thermo}} - P_{\text{mech}})$ reaches its right value corresponding to the present thermodynamic state, the system will move to another thermodynamic state at which $(P_{\text{thermo}} - P_{\text{mech}})$ significantly differs from that of previous one. In this way, system will never be able to achieve correct value of $(P_{\text{thermo}} - P_{\text{mech}})$. Hence, the instantaneous value of $(P_{\text{thermo}} - P_{\text{mech}})/\nabla \cdot \vec{u}$ will not represent μ_b. For this simulation ($\nabla \cdot \vec{u} = 10^8\ \text{s}^{-1}$), we have observed $\Delta\mu_b$ to be less than 3×10^{-7} Pa s in a time interval of length $\tau_{\text{rot}} = 0.53$ ns. Therefore, we can neglect the effects of continuously varying μ_b and take the instantaneous value of $(P_{\text{thermo}} - P_{\text{mech}})/\nabla \cdot \vec{u}$ as the bulk viscosity at the prevailing temperature and pressure.

Figure 8 compares the PV graph for the expansion and compression processes. Hysteresis is formed due to nonisentropicity caused by bulk viscosity. For a given volume and total kinetic energy of the system, the mechanical pressure during compression is greater than the mechanical pressure during the expansion process. Therefore, after a complete cycle of expansion and compression for a duration of 15 ns each, there is a net input of energy into the system by means of PV work. Since a sound wave is a wave of compression and expansion, the above-mentioned mechanism also explains the role of bulk viscosity in the absorption of sound wave at a microscopic level, i.e., how bulk viscosity causes some part of sound energy to convert into thermal energy of the gas after each cycle of compression and expansion.

1. Contribution of pairwise interaction in pressure

Figure 9 shows the variation in the absolute value of contribution of intermolecular interaction (P_{pair}) to pressure during the simulation and compares it with instantaneous kinetic (mechanical) pressure. P_{pair} is negative due to the attractive nature of intermolecular interactions at large distances corresponding to the dilute gas conditions. As the expansion begins, the contribution of intermolecular interaction (P_{pair}) in pressure calculation decreases due to increase in intermolecular distances and vice versa for compression.

In the present study, the gas is in a dilute state, since the density of the system remains between 0.1865 and 0.8358 kg/m^3 throughout the simulation. Corresponding number densities are 4.0×10^{24} and 1.8×10^{25} m^{-3}. Accordingly, the contribution to pressure due to pairwise intermolecular interaction, P_{pair}, remains less than 0.04% of the kinetic pressure throughout the simulation. It can be observed from Fig. 9 that the maximum value of P_{pair} is 20 Pa, which is indeed very small as compared to $P_{\text{kinetic}} \approx 10^5$ Pa. Therefore, we have neglected the contribution of pairwise intermolecular interaction (P_{pair}) in the calculation of pressure and accounted for only the contribution of kinetic energy to the calculation of P_{mech} and P_{thermo}. Moreover, the calculation of bulk viscosity in this method depends on the difference $P_{\text{mech}} - P_{\text{thermo}}$ rather than the individual values of P_{mech} and P_{thermo}. By definition, both the P_{mech} and P_{thermo} correspond to same volume and same density, and therefore, for a dilute gas, the contribution of P_{pair} to both P_{mech} and P_{thermo} should be almost the same. Because of this reason, the contribution of P_{pair} would get nullified in the calculation of bulk viscosity.

This enables us to ignore the contribution of intermolecular forces to the bulk viscosity.

2. Compression followed by expansion

Now we study the impact of the order of expansion and compression processes on the bulk viscosity, i.e., if

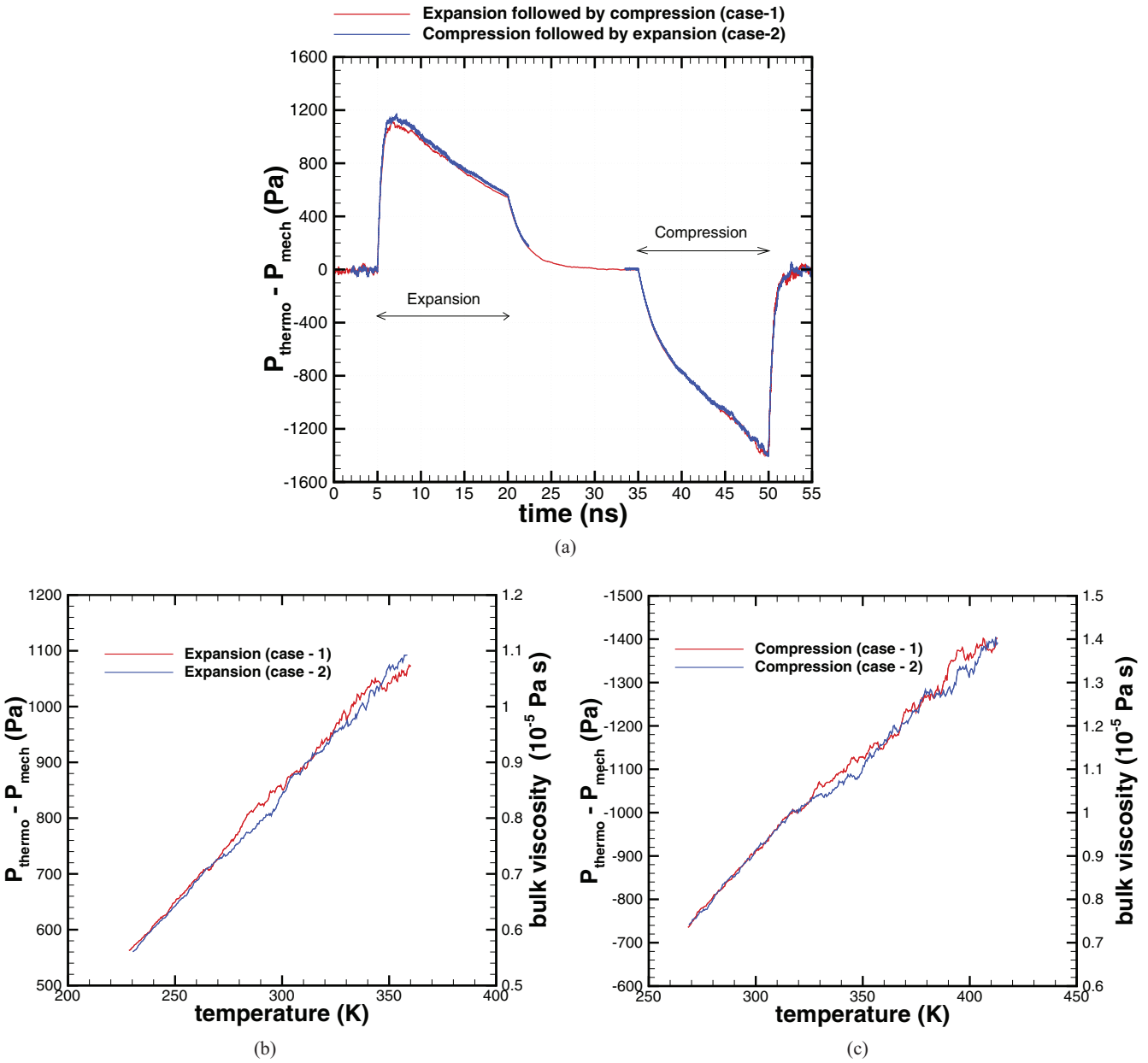

FIG. 10. (a) Comparison of $P_{\text{thermo}} - P_{\text{mech}}$ vs. time for the two cases. In case 1, fluid is first expanded and then compressed, whereas in case 2, the fluid is first compressed and then expanded. To ease the comparison between these two cases, the expansion and compression parts of case 2 are separated and superimposed on the corresponding parts of case 1 curve. Panels (b) and (c) show the comparison of variation of $P_{\text{thermo}} - P_{\text{mech}}$ and μ_b vs. temperature during expansion and compression, respectively, for both the cases.

compression is performed before the expansion, rather than first expansion and then compression. We have studied these two cases and results are discussed as follows. The first case, case 1, is the simulation discussed in Fig. 4, in which system is subjected to following processes in the order of mention—equilibration, expansion, equilibration, compression, and a final equilibration. In case 2, the order of processes is reversed. In this case, a new system is created and equilibrated at temperature and pressure corresponding to that of case 1 at $t = 35$ ns. Next, it is compressed for 15 ns and then again equilibrated for 15 ns. After that the system is expanded for 15 ns. Finally, in the end it is again equilibrated.

Results are shown in Fig. 10(a). In this figure, to ease the comparison between these two cases, the expansion and compression parts of case 2 are separated and superimposed on the corresponding parts of case 1 curve. In this figure, it can be observed that both the curves are overlapping in case of compression. However, for expansion, case 2 shows slightly higher values of $P_{\text{thermo}} - P_{\text{mech}}$, although the difference is still less than 2.5%. This small difference can be explained as follows: Although the volume of the system is same, the energy content, and hence temperature, of case 1 at $t = 55$ ns is higher than that at $t = 0$ ns, as it has undergone an irreversible cycle of expansion and compression. Since the compression of case 2 is started from the same thermodynamic state of

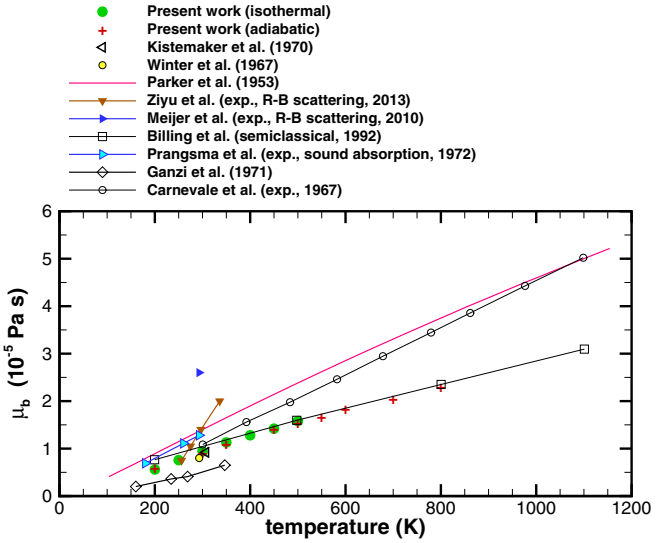

FIG. 11. Variation of bulk viscosity, μ_b, with temperature at pressure of 1 bar.

case 1 at $t = 35$ ns, after the compression of same duration (15 ns), the case 2 has the same temperature as that of case 1 at 55 ns. Therefore, the temperature of case 2 just before the expansion is slightly higher than that of case 1. Therefore, because of higher temperature at any corresponding time step, the $\mu_b \nabla \cdot \vec{u}$, and hence $P_{\text{thermo}} - P_{\text{mech}}$ in case 2, is found to be slightly higher than that in case 1.

Figures 10(b) and 10(c) compare the plots of $P_{\text{thermo}} - P_{\text{mech}}$ and bulk viscosity with respect to temperature for cases 1 and 2 for expansion and compression processes, respectively. It is quite evident that $P_{\text{thermo}} - P_{\text{mech}}$ and bulk viscosity values are in a very good agreement between the two cases.

C. Variaton of bulk viscosity with temperature and pressure

Figure 11 shows variation of bulk viscosity with temperature. The simulations are carried out at $\nabla \cdot \vec{u} = 10^8$ s^{-1}. Noteworthy is the fact that only limited data are available for bulk viscosity in literature. Therefore, in addition to this directly available data, we have also used data available for rotational collision number (Z_{rot}) to calculate bulk viscosity using Tisza's relation [3]. A comparison of data collected from literature in this manner with our results is made in Fig. 11. It should also be noted that each of the data point, corresponding to the present work, shown in the Fig. 11 is obtained using a separate numerical experiment. Each simulation took approximately 96 h of computations on 120 Intel Xeon 2.5-GHz processors. It can be observed that the available experimental or numerical values for the bulk viscosity of nitrogen are spread over a wide range, as they have been obtained by different researchers and using different methods. Our results also fall in that range and closely match with the results of Billing *et al.* [68], who used a semiclassical model to calculate rotational collision number by treating rotational motion in classical fashion and vibrational relaxation in a nonclassical quantized manner. Our results also match closely with experimental data of Winter *et al.* [46] and Kistemaker *et al.* [71]. It should be noted that experiments used for determination of bulk viscosity rely on indirect methods, like absorption and dispersion of sound or Rayleigh-Brillouin scattering. In contrast to this, the method proposed in this work has a strong theoretical basis and gives the estimation of bulk viscosity from a direct assessment of the difference between mechanical and thermodynamic pressure [52,70–72,76].

After studying the variation of bulk viscosity with temperature, our next aim is to study its variation with pressure. For this purpose, we have simulated isothermal expansion by adding Nose-Hoover thermostat in our MD simulations. Since, in an isothermal expansion, only pressure changes and the temperature remains constant, the observed variation of bulk viscosity can be attributed to pressure alone. However, a thermostat is a computational trick to maintain a constant temperature in a simulation. Therefore, to avoid any computational artifacts in the simulation, it is necessary to ensure that the thermostat does not interfere with the natural relaxation of the gas, i.e., it does not alter the dynamics of system in a way that is unrealistic or inconsistent with the natural physics. Therefore, we have first verified that both the adiabatic and isothermal expansion yield same bulk viscosity (within the limits of statistical error of simulation) at a given temperature and pressure. This can be seen from our data for isothermal and adiabatic expansion in Fig. 11. Another reason for comparing bulk viscosity obtained from adiabatic expansion to isothermal one is as follows: A natural expansion of gas caused by the flow over an aerodynamic object in an open atmosphere with $\nabla \cdot \vec{u} = 10^8$ s^{-1} resembles more an adiabatic rather than isothermal expansion. Because, to maintain a constant temperature, fluid needs to be thermally equilibrated with its surrounding. However, this process of equilibration is not instantaneous and requires some finite time. When the fluid is expanded or compressed at $\nabla \cdot \vec{u}$ of the order of 10^8 s^{-1}, the temperature of gas changes so rapidly that flow does not get enough time for a significant energy exchange with the surrounding, and hence such flow conditions resemble more to adiabatic rather than isothermal conditions.

Figure 12 shows the variation of bulk viscosity with pressure at temperature values of 200, 350, and 500 K. Each of these three isotherms is an average of four independent trajectories, each done with 70 million N_2 molecules. The fluctuation of the curve can be reduced by further increasing the number of molecules in the simulation or by taking the average over more trajectories. It can be observed that at lower pressures, bulk viscosity decreases with pressure. The probable reason for this trend is that at as the pressure decreases, the rotational relaxation time increases, and at very low pressures the characteristic time of flow starts becoming comparable to relaxation time. However, as the pressure increases, this dependence gradually weakens, and beyond some range, the bulk viscosity can be assumed as independent of pressure.

Now we provide an estimate for error involved in the calculation of bulk viscosity using the proposed method. Figure 13 shows the four different trajectories for variation of bulk viscosity with pressure at a constant temperature of 350 K in the plateau region of 1 to 2 bar (see Fig. 12). Each of the trajectories was started with microscopically different but macroscopically same initial condition. It can be observed that for more than 95% of the times, bulk viscosity fluctuations lie in $(1.123 \pm 0.05) \times 10^{-5}$ Pa s. Standard deviation and

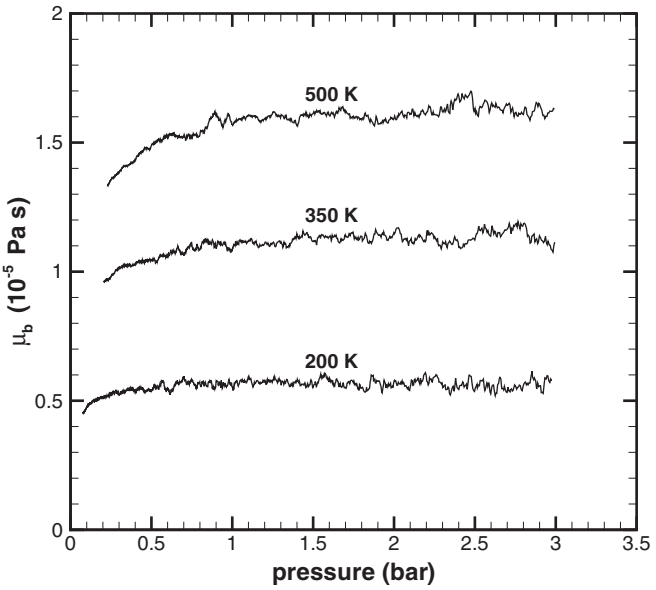

FIG. 12. Variation of bulk viscosity with pressure.

standard error for the curve showing average of these four trajectories are 1.2×10^{-7} and 1.0×10^{-8} Pa s, respectively. For the other two curves of 200 K and 500 K (Fig. 12), standard deviations are 1.3×10^{-7} and 1.5×10^{-7} Pa s, respectively, while the corresponding standard errors are 9.3×10^{-9} and 1.1×10^{-8} Pa s. We have observed similar range of uncertainty in all the values of bulk viscosity reported in this work.

D. Variation of bulk viscosity with $\nabla \cdot \vec{u}$

Although dependence of bulk viscosity on the frequency of sound is studied in a few works [46], to the best of our knowledge, a direct study of the dependence of bulk viscosity on $\nabla \cdot \vec{u}$ has not been done so far. The reason for this is that

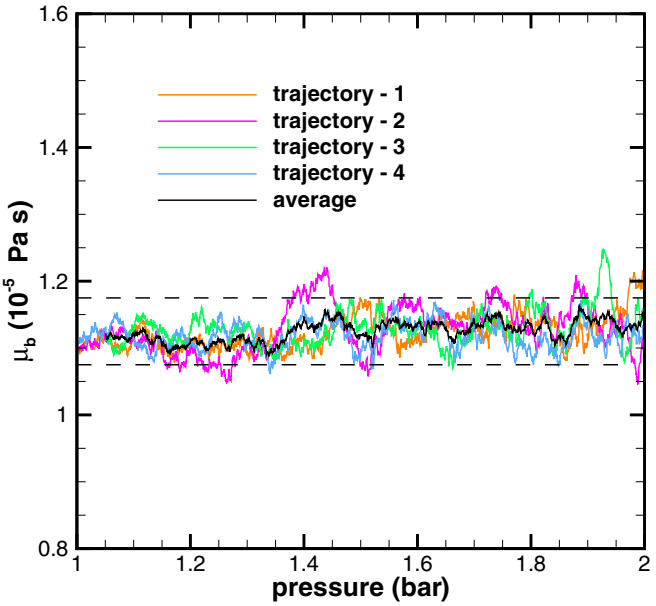

FIG. 13. Four different trajectories for variation of bulk viscosity with pressure at a constant temperature of 350 K in the plateau region of 1 to 2 bar (see Fig. 12).

carrying out such an experiment is difficult to perform [4], and available numerical methods (i.e., the Green-Kubo method and Einstein's method) are unable to simulate expansion or compression, since they are based on equilibrium molecular dynamics (see Sec. III). However, the method proposed in this work, being inherently based on expansion and compression of the gas, enables us to investigate the effects of $\nabla \cdot \vec{u}$ on bulk viscosity.

The equation of sound wave $[P - P_{\rm eq} = (P - P_{\rm eq})_{\rm max} \sin(\omega t)]$ combined with the adiabatic relation $(P\mathcal{V}^{\gamma} = \text{constant})$ yields

$$\frac{1}{\mathcal{V}}\frac{d\mathcal{V}}{dt} = \nabla \cdot \vec{u} = -\frac{\omega}{\gamma}\frac{(P - P_{\rm eq})_{\rm max}}{P}\cos(\omega t). \tag{21}$$

If we consider conditions of a typical sound absorption experiment, $(P - P_{\rm eq})_{\rm max} \sim 10^{-2}$ Pa, $P \sim 10^5$ Pa, $\gamma = 1.4$, and $\omega = 100$ MHz, then we get $\nabla \cdot \vec{u}$ of the order of 10. On the other hand, in practical situations where it is important to account for bulk viscosity effect, e.g., supersonic and hypersonic flows, $\nabla \cdot \vec{u}$ may be of the order of 10^5 $\rm s^{-1}$. Therefore, in analysis of such situations, the use of bulk viscosity calculated by the sound absorption and dispersion method is questionable.

Also, in case of higher-frequency sound waves at high temperatures with activated vibrational modes, if $1/\omega$ becomes very small as compared to relaxation time ($\tau_{\rm vib}$) of vibrational mode, i.e., $(1/\omega\tau_{\rm vib}) \ll 1$, then $\nabla \cdot \vec{u}$ changes its sign so frequently that system does not get enough time for any significant exchange of energy to take place between the vibrational mode and other modes of energy. Therefore, at higher frequencies (gigahertz range), the vibrational mode effectively behaves as frozen and only internal modes with shorter relaxation time, viz., rotational mode, contribute to the relaxation process [52]. Whereas if the system is subjected to a steady compression or expansion with constant $\nabla \cdot \vec{u}$, there will be plenty of time for all internal modes to participate in the energy exchange process, and hence both vibrational and rotational modes contribute to the bulk viscosity at all values of $\nabla \cdot \vec{u}$. Therefore, for applications in high-divergence steady-state flows, the value of bulk viscosity computed by the proposed method should be used rather than those calculated by sound absorption and dispersion or optical methods.

As mentioned earlier, although Eq. (3) is in principle applicable to all expansion and compression rates, the practical application of the proposed approach requires a sufficiently high expansion or compression rate. The reason for this is as follows: The Eq. (3), $P_{\rm mech} - P_{\rm thermo} = \mu_b \nabla \cdot \vec{u}$, suggests that for a given thermodynamic state of the fluid, i.e., for a given μ_b, higher $\nabla \cdot \vec{u}$ results in greater $P_{\rm mech} - P_{\rm thermo}$. Since $\nabla \cdot \vec{u}$ is a controlled variable in the simulation, the statistical error in estimated bulk viscosity, μ_b, is directly related to statistical error in calculated $P_{\rm mech} - P_{\rm thermo}$, which in turn depends on statistical fluctuations of $P_{\rm mech}$ and $P_{\rm thermo}$. Thus, in order to minimize the statistical error in measured bulk viscosity, it is desired that the signal, $P_{\rm mech} - P_{\rm thermo}$, is at least an order of magnitude greater than the statistical fluctuations in the $P_{\rm mech}$ and $P_{\rm thermo}$. Hence, sufficiently high expansion and compression rates are required. One can reduce these statistical fluctuations either by increasing number of

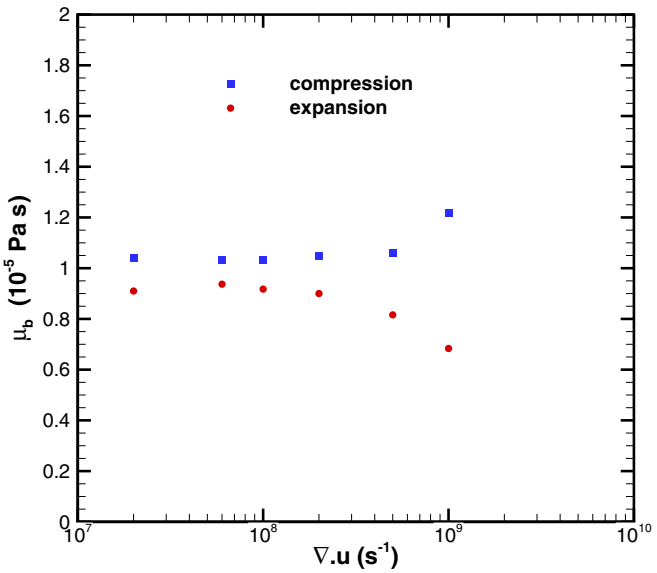

FIG. 14. Variation of bulk viscosity with $\nabla \cdot \vec{u}$ at 300 K.

simulated molecules or by taking average over several independent molecular dynamics trajectories.

However, it should also be noted that the bulk viscosity is a thermodynamic parameter only if the deviation of the system from local thermodynamic equilibrium is small. At higher deviation, bulk viscosity will depend not only on the thermodynamic state of the system, i.e., temperature and pressure, but also on the expansion and compression rates. Therefore, a too-high value of $\nabla \cdot \vec{u}$ should also be avoided. In summary, the smallest possible value of $\nabla \cdot \vec{u}$ is desired, which can produce $P_{\text{mech}} - P_{\text{thermo}}$ large enough such that its statistical fluctuations are small. In case of N_2, we found $\nabla \cdot \vec{u} = 10^8$ s^{-1} to be a reasonably good choice.

The above-mentioned constraints restrict us to use values of $|\nabla \cdot \vec{u}|$ greater than 2×10^7. For the allowed range of expansion or compression rates, the variation of μ_b with $\nabla \cdot \vec{u}$ at 300 K is presented in Fig. 14. The graph shows that bulk viscosity remains roughly constant in the range $|\nabla \cdot \vec{u}| = 2 \times 10^7$ to 10^8 s^{-1}. Beyond that, it gradually increases for compression, whereas decreases gradually for the expansion process. It can be observed from Fig. 14 that the bulk viscosity calculated from the compression is slightly higher than that obtained from expansion. This difference is in line with the observations made by Valentini *et al.* [31]. In their molecular dynamics study, they found that the value of Z_{rot} depends not only on the magnitude of nonequilibrium but also on the direction of deviation from equilibrium, i.e., whether the rotational temperature is greater than the translational temperature or otherwise.

VI. CONCLUSIONS

A method based on the continuous compression and expansion of a dilute gas is proposed for the calculation of bulk viscosity, which is one of the most fundamental as well as a critically important fluid property in some situations. The basic idea is to use the classical molecular dynamics approach for the estimation of mechanical and thermodynamic pressures of a gas dilating at a controlled rate. The simulated pressure values are then used to calculate the bulk viscosity, which is found to be in reasonably good agreement with the previous experimental and numerical data available in the literature. The simple, but theoretically sound, method proposed here thus can be used to accurately calculate the bulk viscosity of unknown fluids with much ease using existing molecular models. The method can also be used as an alternative way for calculating rotational collision number of dilute gases.

ACKNOWLEDGMENTS

The authors are thankful to Professor Tapan K. Sengupta of the Department of Aerospace Engineering at the Indian Institute of Technology (IIT) Kanpur for the initial motivation and discussion on the subject of the present work. The authors also acknowledge the use of the High Performance Computing Facility at the Computer Center, IIT Kanpur for carrying out computations required for this work.

[1] G. G. Stokes, On the theories of the internal friction of fluids in motion, Trans. Camb. Phil. Soc. **8**, 287 (1845).
[2] M. Hak Gad-el, Questions in fluid mechanics: Stokes' hypothesis for a Newtonian, isotropic fluid, J. Fluids Eng. **117**, 5 (1995).
[3] L. Tisza, Supersonic absorption and Stokes' viscosity relation, Phys. Rev. **61**, 531 (1942).
[4] C. Truesdell, The present status of the controversy regarding the bulk viscosity of fluids, Proc. R. Soc. Lond. A **226**, 59 (1954).
[5] G. Emanuel, Effect of bulk viscosity on a hypersonic boundary layer, Phys. Fluids A **4**, 491 (1992).
[6] H. Gonzalez and G. Emanuel, Effect of bulk viscosity on Couette flow, Phys. Fluids A **5**, 1267 (1993).
[7] G. Emanuel and B. M. Argrow, Linear dependence of the bulk viscosity on shock wave thickness, Phys. Fluids **6**, 3203 (1994).
[8] J. C. Orou and J. A. Johnson III, Second viscosity enhancement in turbulent nonequilibrium flow, Phys. Fluids **6**, 415 (1994).
[9] K. Xu and E. Josyula, Continuum formulation for non-equilibrium shock structure calculation, Commun. Comput. Phys. **1**, 425 (2006).
[10] T. G. Elizarova, A. A. Khokhlov, and S. Montero, Numerical simulation of shock wave structure in nitrogen, Phys. Fluids **19**, 068102 (2007).
[11] G. Fru, G. Janiga, and D. Thévenin, Impact of volume viscosity on the structure of turbulent premixed flames in the thin reaction zone regime, Flow, Turbul. Combust. **88**, 451 (2012).
[12] M. Cramer and F. Bahmani, Effect of large bulk viscosity on large-Reynolds-number flows, J. Fluid Mech. **751**, 142 (2014).
[13] F. Bahmani and M. Cramer, Suppression of shock-induced separation in fluids having large bulk viscosities, J. Fluid Mech. **756**, R2 (2014).

[14] A. Chikitkin, B. Rogov, G. Tirsky, and S. Utyuzhnikov, Effect of bulk viscosity in supersonic flow past spacecraft, Appl. Numer. Math. **93**, 47 (2015).

[15] T. K. Sengupta, A. Sengupta, N. Sharma, S. Sengupta, A. Bhole, and K. Shruti, Roles of bulk viscosity on Rayleigh-Taylor instability: Non-equilibrium thermodynamics due to spatio-temporal pressure fronts, Phys. Fluids **28**, 094102 (2016).

[16] S. Singh and R. Myong, A computational study of bulk viscosity effects on shock-vortex interaction using discontinuous Galerkin method, Korea Soc. Comput. Fluids Eng. **22**, 86 (2017).

[17] J. Lin, C. Scalo, and L. Hesselink, Bulk viscosity model for near-equilibrium acoustic wave attenuation, arXiv:1707.05876.

[18] S. J. Marcy, Evaluating the second coefficient of viscosity from sound dispersionor absorption data, AIAA J. **28**, 171 (1990).

[19] W. G. Hoover, A. J. Ladd, R. B. Hickman, and B. L. Holian, Bulk viscosity via nonequilibrium and equilibrium molecular dynamics, Phys. Rev. A **21**, 1756 (1980).

[20] L. D. Landau and E. M. Lifshitz, *Course of Theoretical Physics - Fluid Mechanics* (Elsevier, Amsterdam, 2013).

[21] M. S. Cramer, Numerical estimates for the bulk viscosity of ideal gases, Phys. Fluids **24**, 066102 (2012).

[22] G. Buresti, A note on Stokes' hypothesis, Acta Mech. **226**, 3555 (2015).

[23] R. F. Sawyer, Bulk viscosity of hot neutron-star matter and the maximum rotation rates of neutron stars, Phys. Rev. D **39**, 3804 (1989).

[24] H. Dong, N. Su, and Q. Wang, Bulk viscosity in nuclear and quark matter, J. Phys. G: Nucl. Part. Phys. **34**, S643 (2007).

[25] N. S. Demir, Extraction of Hot QCD Matter Transport Coefficients Utilizing Microscopic Transport Theory, Ph.D. thesis, Duke University, 2010.

[26] K. Herzfeld and F. Rice, Dispersion and absorption of high frequency sound waves, Phys. Rev. **31**, 691 (1928).

[27] H. Okumura and F. Yonezawa, New formula for the bulk viscosity constructed from the interatomic potential and the pair distribution function, J. Chem. Phys. **116**, 7400 (2002).

[28] G. J. Prangsma, A. H. Alberga, and J. Beenakker, Ultrasonic determination of the volume viscosity of N_2, CO, CH_4 and CD_4 between 77 and 300 K, Physica **64**, 278 (1973).

[29] S. Chapman, T. G. Cowling, and D. Burnett, *The Mathematical Theory of Non-uniform Gases: An Account of the Kinetic Theory of Viscosity, Thermal Conduction and Diffusion in Gases* (Cambridge University Press, Cambridge, 1990).

[30] V. Istomin, and E. Kustova, Transport coefficients and heat fluxes in non-equilibrium high-temperature flows with electronic excitation, Phys. Plasmas **24**, 022109 (2017).

[31] P. Valentini, C. Zhang, and T. E. Schwartzentruber, Molecular dynamics simulation of rotational relaxation in nitrogen: Implications for rotational collision number models, Phys. Fluids **24**, 106101 (2012).

[32] D. W. v. Oertzen, Transport Coefficients in Quantum Chromodynamics, Ph.D. thesis, University of Cape Town, 1990.

[33] K. Saha, S. Ghosh, and S. Upadhaya, A comparative study of Bulk Viscosity of strongly interacting systems, DAE Symp. Nucl. Phys. **62**, 944 (2017).

[34] S. Gavin, Transport coefficients in ultra-relativistic heavy-ion collisions, Nucl. Phys. A **435**, 826 (1985).

[35] M. Prakash, M. Prakash, R. Venugopalan, and G. Welke, Non-equilibrium properties of hadronic mixtures, Phys. Rep. **227**, 321 (1993).

[36] M. Prakash, M. Prakash, R. Venugopalan, and G. M. Welke, How Fast is Equilibration in Hot Hadronic Matter? Phys. Rev. Lett. **70**, 1228 (1993).

[37] S. De Groot, W. van Leeuwen, and G. van Weert Ch, *Relativistic Kinetic Theory: Principles and Applications* (North-Holland, Amsterdam, 1980).

[38] P. Chakraborty and J. I. Kapusta, Quasiparticle theory of shear and bulk viscosities of hadronic matter, Phys. Rev. C **83**, 014906 (2011).

[39] N. Demir and S. A. Bass, Extracting hadronic viscosity from microscopic transport models, Eur. Phys. J. C **62**, 63 (2009).

[40] N. Demir and S. A. Bass, Shear-Viscosity to Entropy-Density Ratio of a Relativistic Hadron Gas, Phys. Rev. Lett. **102**, 172302 (2009).

[41] W. E. Meador, G. A. Miner, and L. W. Townsend, Bulk viscosity as a relaxation parameter: Fact or fiction? Phys. Fluids **8**, 258 (1996).

[42] X.-D. Li, Z.-M. Hu, and Z.-L. Jiang, Continuum perspective of bulk viscosity in compressible fluids, J. Fluid Mech. **812**, 966 (2017).

[43] A. H. M. Zaheri, S. Srivastava, and K. Tankeshwar, Theoretical evaluation of bulk viscosity: Expression for relaxation time, Phys. Rev. E **76**, 041204 (2007).

[44] R. E. Graves and B. M. Argrow, Bulk viscosity: Past to present, J. Thermophys. Heat Transfer **13**, 337 (1999).

[45] S. Karim and L. Rosenhead, The second coefficient of viscosity of liquids and gases, Rev. Mod. Phys. **24**, 108 (1952).

[46] T. G. Winter and G. L. Hill, High-Temperature ultrasonic measurements of rotational relaxation in hydrogen, deuterium, nitrogen, and oxygen, J. Acoust. Soc. Am. **42**, 848 (1967).

[47] X. Pan, M. N. Shneider, and R. B. Miles, Power spectrum of coherent Rayleigh-Brillouin scattering in carbon dioxide, Phys. Rev. A **71**, 045801 (2005).

[48] X. Pan, M. N. Shneider, and R. B. Miles, Coherent Rayleigh-Brillouin scattering in molecular gases, Phys. Rev. A **69**, 033814 (2004).

[49] M. O. Vieitez, E. J. Van Duijn, W. Ubachs, B. Witschas, A. Meijer, A. S. De Wijn, N. J. Dam, and W. Van de Water, Coherent and spontaneous Rayleigh-Brillouin scattering in atomic and molecular gases and gas mixtures, Phys. Rev. A **82**, 043836 (2010).

[50] Z. Gu and W. Ubachs, Temperature-dependent bulk viscosity of nitrogen gas determined from spontaneous Rayleigh–Brillouin scattering, Optics Lett. **38**, 1110 (2013).

[51] Z. Gu and W. Ubachs, A systematic study of Rayleigh-Brillouin scattering in air, N_2, and O_2 gases, J. Chem. Phys. **141**, 104320 (2014).

[52] A. Meijer, A. de Wijn, M. Peters, N. Dam, and W. van de Water, Coherent Rayleigh–Brillouin scattering measurements of bulk viscosity of polar and nonpolar gases, and kinetic theory, J. Chem. Phys. **133**, 164315 (2010).

[53] A. S. Dukhin and P. J. Goetz, Bulk viscosity and compressibility measurement using acoustic spectroscopy, J. Chem. Phys. **130**, 124519 (2009).

[54] M. S. Green, Markoff random processes and the statistical mechanics of time-dependent phenomena. II. Irreversible processes in fluids, J. Chem. Phys. **22**, 398 (1954).

[55] R. Kubo, Statistical-mechanical theory of irreversible processes. I. General theory and simple applications to magnetic and conduction problems, J. Phys. Soc. Jpn. **12**, 570 (1957).

[56] Y. Zhang, A. Otani, and E. J. Maginn, Reliable viscosity calculation from equilibrium molecular dynamics simulations: A time decomposition method, J. Chem. Theory Comput. **11**, 3537 (2015).

[57] D. C. Rapaport, *The Art of Molecular Dynamics Simulation* (Cambridge University Press, Cambridge, 2004).

[58] M. P. Allen and D. J. Tildesley, *Computer Simulation of Liquids* (Oxford University Press, Oxford, 2017).

[59] S. Plimpton, Fast parallel algorithms for short-range molecular dynamics, J. Comp. Phys. **117**, 1 (1995).

[60] T. Tokumasu and Y. Matsumoto, Dynamic molecular collision (DMC) model for rarefied gas flow simulations by the DSMC method, Phys. Fluids **11**, 1907 (1999).

[61] D. R. Lide, *CRC Handbook of Chemistry and Physics, 89th ed.* (CRC Press, Boca Ration, FL, 2009).

[62] G. Emanuel, Bulk viscosity of a dilute polyatomic gas, Phys. Fluids A **2**, 2252 (1990).

[63] H. C. Andersen, Rattle: A "velocity" version of the shake algorithm for molecular dynamics calculations, J. Comput. Phys. **52**, 24 (1983).

[64] D. M. Heyes, Pressure tensor of partial-charge and point-dipole lattices with bulk and surface geometries, Phys. Rev. B **49**, 755 (1994).

[65] T. W. Sirk, S. Moore, and E. F. Brown, Characteristics of thermal conductivity in classical water models, J. Chem. Phys. **138**, 064505 (2013).

[66] A. P. Thompson, S. J. Plimpton, and W. Mattson, General formulation of pressure and stress tensor for arbitrary many-body interaction potentials under periodic boundary conditions, J. Chem. Phys. **131**, 154107 (2009).

[67] H. J. Hanley and J. F. Ely, The viscosity and thermal conductivity coefficients of dilute nitrogen and oxygen, J. Phys. Chem. Ref. Data **2**, 735 (1973).

[68] G. D. Billing and L. Wang, Semiclassical calculations of transport coefficients and rotational relaxation of nitrogen at high temperatures, J. Phys. Chem. **96**, 2572 (1992).

[69] E. Vogel, Präzisionsmessungen des Viskositätskoeffizienten von Stickstoff und den Edelgasen zwischen Raumtemperatur und 650 K, Ber. Bunsengesellsch. physik. Chem. **88**, 997 (1984).

[70] J. G. Parker, C. Adams, and R. Stavseth, Absorption of sound in argon, nitrogen, and oxygen at low pressures, J. Acoust. Soc. Am. **25**, 263 (1953).

[71] P. Kistemaker, A. Tom, and A. D. Vries, Rotational relaxation numbers for the isotopic molecules of N_2 and CO, Physica **48**, 414 (1970).

[72] E. Carnevale, C. Carey, and G. Larson, Ultrasonic determination of rotational collision numbers and vibrational relaxation times of polyatomic gases at high temperatures, J. Chem. Phys. **47**, 2829 (1967).

[73] G. Ganzi and S. I. Sandler, Determination of thermal transport properties from thermal transpiration measurements, J. Chem. Phys. **55**, 132 (1971).

[74] C. Nyeland and G. D. Billing, Transport coefficients of diatomic gases: Internal-state analysis for rotational and vibrational degrees of freedom, J. Phys. Chem. **92**, 1752 (1988).

[75] D. Bruno and V. Giovangigli, Relaxation of internal temperature and volume viscosity, Phys. Fluids **23**, 093104 (2011).

[76] Y. Fujii, R. Lindsay, and K. Urushihara, Ultrasonic absorption and relaxation times in nitrogen, oxygen, and water vapor, J. Acoust. Soc. Am. **35**, 961 (1963).